ACS APPLIED MATERIALS & INTERFACES
Research Article
www.acsami.org

Hollow Fluffy Co_3O_4 Cages as Efficient Electroactive Materials for Supercapacitors and Oxygen Evolution Reaction

Xuemei Zhou,[†] Xuetao Shen,[†] Zhaoming Xia,[†] Zhiyun Zhang,[†] Jing Li,[†] Yuanyuan Ma,[*,†] and Yongquan Qu[*,†,‡]

[†]Center for Applied Chemical Research, Frontier Institute of Science and Technology, and State Key Laboratory for Mechanical Behavior of Materials, Xi'an Jiaotong University and [‡]MOE Key Laboratory for Nonequilibrium Synthesis and Modulation of Condensed Matter, Xi'an Jiaotong University, Xi'an 710049, China

S *Supporting Information*

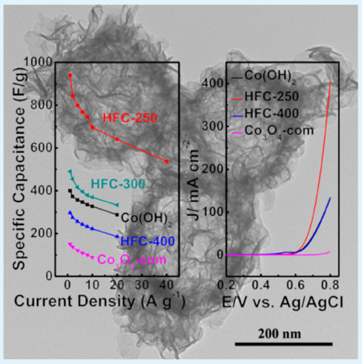

ABSTRACT: Nano-/micrometer multiscale hierarchical structures not only provide large surface areas for surface redox reactions but also ensure efficient charge conductivity, which is of benefit for utilization in areas of electrochemical energy conversion and storage. Herein, hollow fluffy cages (HFC) of Co_3O_4, constructed of ultrathin nanosheets, were synthesized by the formation of $Co(OH)_2$ hollow cages and subsequent calcination at 250 °C. The large surface area (245.5 $m^2\ g^{-1}$) of HFC Co_3O_4 annealed at 250 °C ensures the efficient interaction between electrolytes and electroactive components and provides more active sites for the surface redox reactions. The hierarchical structures minimize amount of the grain boundaries and facilitate the charge transfer process. Thin thickness of nanosheets (2−3 nm) ensures the highly active sites for the surface redox reactions. As a consequence, HFC Co_3O_4 as the supercapacitor electrode exhibits a superior rate capability, shows an excellent cycliability of 10 000 cycles at 10 A g^{-1}, and delivers large specific capacitances of 948.9 and 536.8 F g^{-1} at 1 and 40 A g^{-1}, respectively. Catalytic studies of HFC Co_3O_4 for oxygen evolution reaction display a much higher turnover frequency of $1.67 \times 10^{-2}\ s^{-1}$ in pH 14.0 KOH electrolyte at 400 mV overpotential and a lower Tafel slope of 70 mV dec^{-1}. HFC Co_3O_4 with the efficient electrochemical activity and good stability can remain a promising candidate for the electrochemical energy conversion and storage.

KEYWORDS: *hollow cages Co_3O_4, hierarchical structures, ultrathin nanosheets, electrochemical capacitance, oxygen evolution reaction*

1. INTRODUCTION

Facing increasing energy challenges and environmental pollution, there is an urgent need to seek efficient, clean, and sustainable sources of energy as well as new technologies for energy conversion and storage.[1−8] Transitional metal oxides/hydroxides exhibit potential applications for energy conversion and storage because of the reversible surface redox reactions.[5,9−12] Particularly, the first-row transition metal (Fe, Co, Ni, and Mn) compounds have been considered as promising electrode materials for supercapacitors and lithium-ion batteries as well as efficient cocatalysts for water splitting.[5,11,13−30]

Among the transition metal compounds, Co_3O_4 is considered as a promising electroactive material because of its low cost, environmentally benignancy, and high catalytic activity. Many efforts have been devoted to control the synthesis of Co_3O_4 structures with various morphologies including nanoparticles,[31] nanorods,[32,33] nanowires,[34−36] nanosheets,[37,38] and porous nanostructures.[39,40] When explored as the electroactive materials for supercapacitors, the specific capacitance of Co_3O_4 nanostructures is significantly smaller than the theoretical one of 3560 F g^{-1}, especially at high current densities. The available surface area for redox reactions and inefficient charge conductivity at high rates limit the performance of Co_3O_4 electrodes. Recently, many efforts have been placed on the synthesis of Co_3O_4 nanostructures on highly conductive substrates (e.g., carbon fiber paper[41] and nickel foam,[34,42]) in order to improve the performance of electrodes at high rates for supercapacitors. It is still a challenge to optimize the composition and morphology of cobalt-based electroactive materials, which can dramatically improve their performance to achieve large specific capacitance, good capability, and long-term stability at various current densities. To transform the above goals into reality can be achieved by rationally designing the microstructures of the Co_3O_4 materials. In previous reports, the nano-/micrometer hierarchical structures of Co_3O_4 have proven their prowess in energy storage systems because of their benefits of the high conductivity for the charge transfer process.[38,43,44] However, hierarchical Co_3O_4 composed of relatively large nanoparticles reduces the catalytic activity and limits the available surface areas for the desired redox reactions. A possible route to solve this problem is to construct hollow submicrometer structures consisting of ultrathin nanosheets. The submicrometer size can minimize the amount of grain boundaries and improve the charge conductivity. Ultrathin nanosheets can supply large

Received: July 6, 2015
Accepted: August 28, 2015
Published: August 28, 2015

DOI: 10.1021/acsami.5b05989
ACS Appl. Mater. Interfaces 2015, 7, 20322−20331

surface area and more reactive sites with high catalytic activity for the surface redox reactions. Highly porous features also increases accessible channels that facilitate ion diffusion and chemical transfer.

In this work, we successfully obtain submicrometer HFC of Co_3O_4 involving synthesis of hollow $Co(OH)_2$ cages by templating against Cu_2O crystals and subsequent thermal treatments at 250 °C. Such a unique structure constructed by ultrathin nanosheets (2−3 nm) provides a large accessible surface area of 245.5 $m^2\ g^{-1}$ for surface redox reactions and shortens chemical diffusion paths. As a consequence, the HFC of Co_3O_4 as the supercapacitor electrodes exhibit a superior rate capability, deliver a large specific capacitance of 536.8 F g^{-1} at a high rate of 40 A g^{-1}, and show an excellent cycliability over 10 000 cycles at a current density of 10 A g^{-1}. The morphological features of the HFC Co_3O_4 also benefit their catalytic activity toward water oxidation reaction with a high turnover frequency (TOF) of $1.67 \times 10^{-2}\ s^{-1}$ (low bound) and a Tafel slope of 70 mV dec^{-1}.

2. EXPERIMENTAL SECTION

All chemicals are commercially available and used without further purification. Milli-Q water (18.2 MΩ cm) is used for this work.

2.1. Preparation of Cu_2O Template. In a typical synthesis,[45] 20 g of polyvinylpyrrolidone (PVP, M_w = 40 000) was dissolved into an aqueous solution of $CuCl_2 \cdot 2H_2O$ (0.03 M, 400 mL). Then, 50 mL of NaOH aqueous solution (2.7 M) was added dropwise into the above transparent light-blue solution. After stirring for 0.5 h, 10 g of ascorbic acid dissolved in 40 mL of water was added dropwise. A turbid orange liquid gradually formed. The mixture was aged for 3 h. The resulting precipitate was collected by centrifugation, followed by washing with copious amount of water for three times and absolute ethanol for two times to remove the residual inorganic ions and polymer. Finally, the products were dried under vacuum at 60 °C for 5 h.

2.2. Synthesis of HFC $Co(OH)_2$ and Co_3O_4. In a typical procedure,[45] 500 mg of Cu_2O particles and 200 mg of $CoCl_2 \cdot 6H_2O$ were mixed in 500 mL of the ethanol/water (1:1 volumetric ratio) solvent in the presence of 16.67 g of PVP. After continuous stirring for 10 min at room temperature, 200 mL of $Na_2S_2O_3$ (50 g) aqueous solution was added dropwise. Finally, the resulting precipitate was collected by centrifugation, washed with copious amounts of water and absolute ethanol, and dried at 60 °C overnight. The HFC Co_3O_4 was prepared by calcining HFC $Co(OH)_2$ in air for 3 h at various temperature (>250 °C) with a ramp rate of 1 °C/min.

2.3. Characterization. The surface area and pore size were measured by nitrogen physisorption (Micromeritics, ASAP 2020 HD88) on the basis of the Brunauer−Emmet−Teller (BET) method. Thermogravimetric analysis (TGA) of as-synthesized samples were carried out on Mettler Toledo STAR^e at a heating rate of 5 °C min^{-1} from room temperature to 800 °C in air. The phase evolution of as-synthesized nanostructures was monitored by powder X-ray diffraction (XRD). The XRD patterns with diffraction intensity versus 2θ were recorded in a Shimadzu X-ray diffractometer (Model 6000) using Cu Kα radiation. Scanning electron microscopy (SEM) was carried out on Hitachi Su-8010 scanning electron microscope. Transmission electron microscopy (TEM) studies were conducted on a Hitachi HT-7700 transmission electron microscope with an accelerating voltage of 120 kV.

2.4. Electrode Fabrication and Measurements. All electrochemical measurements were recorded by using an electrochemical workstation (CHI 660D, Shanghai, China). The working electrode was prepared from a mixture of the electroactive material HFC Co_3O_4, acetylene black, and polyvinylidenedifluoride (PVDF, Aldrich) blend with a weight ratio of 8:1:1. The electrodes were fabricated by loading the blend onto the surface of nickel foam sheets, drying at 60 °C, and pressing under 10 MPa. The typical loaded mass of the electrode active material was 2−3 mg. KOH (2.0 M) aqueous solution was used as the electrolyte. The capacitive performance of the electrodes was evaluated by using cyclic voltammetry (CV) and chronopotentiometry (CP) measurements at room temperature with a typical three-electrode cell, where Pt foil served as the counter electrode and a Ag/AgCl electrode worked as the reference electrode. The CV measurements were conducted in a potential window of 0−0.45 V versus Ag/AgCl at various scan rates. The constant current charge−discharge test was carried out at various current densities within a potential range of 0 to 0.45 V versus Ag/AgCl. Electrochemical impedance spectroscopy (EIS) was carried out on the AUTOLAB PGSTAT204 electrochemistry workstation in the frequency range from 0.01 Hz to 100 kHz at an open-circuit potential, with 10 mV as the amplitude potential.

2.5. Oxygen Evolution Reaction. Electrocatalytic activities including linear sweep voltammograms (LSV) and chronoamperometry were recorded on a CHI 660D electrochemistry workstation with a standard three-electrode system in pH 14 KOH aqueous solutions. The counter electrode was platinum wire and the reference electrode was standard Ag/AgCl (4 M KCl). The catalyst with a loading of 0.14 mg cm^{-2} on indium tin oxide (ITO) surface was used as the working electrode. The scanning rate for LSV measurements was 50 mV s^{-1}. Rotating-disk electrode voltammograms were obtained at a scan rate of 10 mV s^{-1}.

The generated oxygen was detected by a Thermo Scientific Orion Star A213 Benchtop DO Meter in pH 14 KOH solution. The DO probe was insert into a sealed reactor, together with Pt wire as the counter electrode, Ag/AgCl as the reference electrode, and the catalyst loaded on ITO as the working electrode. Before each experiment, the electrolyte solution was degassed by argon purging to remove dissolved oxygen under strong stirring.

2.6. Calculation of TOF. The values of TOF are calculated from the equation

$$\mathrm{TOF} = (JA)/(4Fm)$$

where J (A cm^{-2}) is the current density at a specified overpotential, A is the area of the ITO electrode, and F is the faraday constant (96 485 C mol^{-1}). The variable m is the number of moles of the active materials loaded onto the ITO.

3. RESULTS AND DISCUSSION

3.1. Synthesis of Hollow Fluffy Submicrometer Cages of Co_3O_4. The synthetic scheme for HFC Co_3O_4 is illustrated in Figure 1a, which involves three steps: synthesis of Cu_2O polyhedras, fabrication of HFC $Co(OH)_2$ precursors by templating against Cu_2O crystals, and formation of HFC Co_3O_4 by the thermal treatments on the as-prepared HFC $Co(OH)_2$.[45] The preparative approach is slightly different from that of previous reports,[45] in which PVP with a large molecular weight (40 000) can induce the formation of the highly fluffy structures instead of the porous cages. Microstructures of as-prepared crystals were examined by TEM and SEM. The TEM image of Cu_2O (Figure 1b) showed a polyhedron structure with a size of ∼250 nm. XRD spectrum given in Figure 1c clearly indicated Cu_2O phase (Powder Diffraction File (PDF) no. 05-0667, International Centre for Diffraction Data (ICDD), 2004) of as-synthesized crystals. The following chemical etching reactions between $Na_2S_2O_3$ and Cu_2O in stiu released hydroxide anions at the interface of liquid and solid, which induced the local precipitation of cobalt ions on the surface of Cu_2O crystal. The general chemical route could be described as follows:

$$Cu_2O + xS_2O_3^{\ 2-} + H_2O \rightarrow [Cu_2(S_2O_3^{\ 2-})_x]^{2-2x} + 2OH^- \quad (1)$$

$$S_2O_3^{\ 2-} + H_2O \rightleftharpoons HS_2O_3^{\ 2-} + OH^- \quad (2)$$

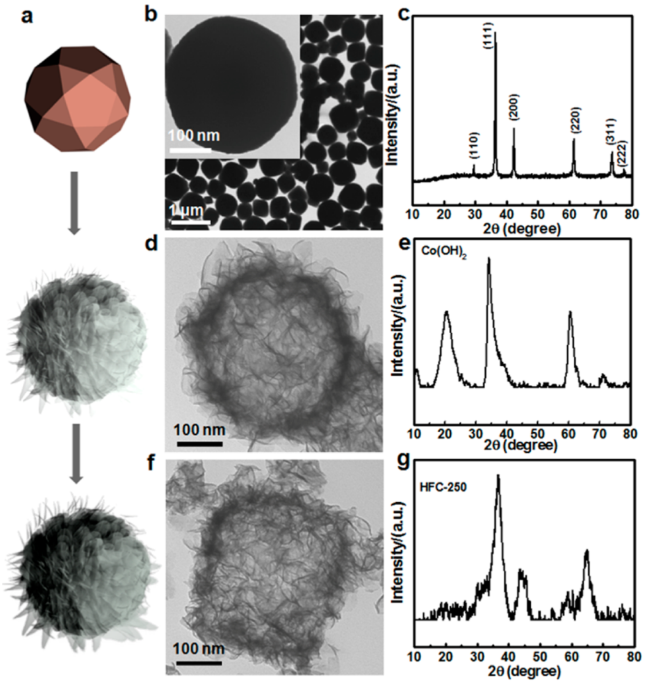

Figure 1. (a) Schematic illustration of the fabrication of $Co(OH)_2$ and Co_3O_4 by thermal treating of $Co(OH)_2$. TEM images for (b) Cu_2O template, (d) $Co(OH)_2$, and (f) Co_3O_4. XRD pattern for (c) Cu_2O template, (e) $Co(OH)_2$, and (g) Co_3O_4.

$$Co^{2+} + 2OH^- \rightarrow Co(OH)_2 \qquad (3)$$

When $Na_2S_2O_3$ is added into the dispersion of Cu_2O crystals, OH^- is released (eqs 1 and 2). Meanwhile, $Co(OH)_2$ starts to precipitate synchronously at the etching interface where the local concentration of OH^- is the highest (eq 3). The synchronous chemical reactions guarantee that the exterior of $Co(OH)_2$ shell perfectly imitates the geometrics of Cu_2O templates. The shell structure can be reserved in the following coordinating etching procedure. The channels for the chemical transport can be created through the interparticle interstitials for the continuous dissolution of Cu_2O. The SEM and TEM images shown in Figures 1d and S1 reveal the hierarchical morphology features of as-synthesized nanostructures, which were HFC-like crystals constructed by thin nanosheets. The nanosheets were highly transparent to the electron beam, as shown in TEM image (Figure 1d), indicating the very small thickness of the nanosheets. The average thickness of the nanosheet was 2.2 ± 0.54 nm, determined by measuring those vertically aligned in TEM images. The size of the internal voids of as-prepared hollow cages is ~250 nm, which inherits the dimensions of the Cu_2O templates. The average size of the HFC is ~300 nm. XRD spectrum (Figure 1e) reveals that the hollow cages can be indexed to α-$Co(OH)_2$ phase (PDF no. 02-0925, ICCD, 2004). The broad peaks of XRD spectrum can be attributed to the ultrathin thickness of the nanosheets.

Similar to the previous reports and TGA results (Figure S2), $Co(OH)_2$ phase could be completely converted into spinel Co_3O_4 phase (PDF no. 42-1467, ICCD, 2004) after the high-temperature annealing in air.[39,45] When the temperature was over 250 °C, the weight variation became negligible (Figure S2). The actual weight loss of the HFC $Co(OH)_2$ derived from the TGA curve is 13.1%, which is very close to the theoretical value (13.6%) of converting $Co(OH)_2$ into Co_3O_4. Hence, the $Co(OH)_2$ HFCs were annealed at 250, 300, and 400 °C. The obtained products are denoted as HFC-x, where x represents the annealing temperature. Figure 1f,g shows the morphologies of HFC-250 after heat treatment and its XRD spectra. It was found that $Co(OH)_2$ was completely converted into Co_3O_4 after 250 °C treatment in air for 3 h. As evidenced from TEM and SEM images (Figures 1f and S1c,d), the morphology of the HFC-like nanostructure was well preserved after high temperature annealing at 250 °C. The thinness of the nanosheets is retained. Broken cages were observed for the nanostructures annealed at 300 °C (Figure S1e,f). When the annealing temperature was 400 °C, collapsed nanostructures were observed (Figure S3a), and the structural features were partly destroyed. The reason may be attributed to the higher-temperature annealing that easily wrecked the ultrathin nanosheets, broke the thin fluffy structure, and induced structural instability.

Such a change was also reflected by their BET surface areas. Nitrogen gas adsorption/desorption isotherm measurements were used to determine surface areas of HFC $Co(OH)_2$ and Co_3O_4. The specific surface area of the HFC-250 was 245.5 m^2 g^{-1}, which was much higher than that of the Co_3O_4 materials previously reported.[37,39] In contrast, the specific surface areas of HFC-300 (120 m^2 g^{-1}) and HFC-400 (67.3 m^2 g^{-1}) was significantly decreased, which further demonstrated the structural instability of HFC treated at higher temperatures and was consistent with TEM and SEM observations (Figures 1, S1, and S3).

3.2. Electrochemical Supercapacitor of HFC Co_3O_4.

The large surface area of HFC can provide more active sites, efficient interaction between the electrolytes and the surface of the electrodes, and benefit the chemical transfer, all of which are desirable for the surface redox reactions in electrochemical applications. Meanwhile, the submicrometer-scaled hollow fluffy structures minimize the amount of grain boundary and increase the conductivity of the electrodes, which can further improve the electric performance of cobalt oxides. Herein, electroactivity of the HFC of Co_3O_4 was evaluated as the electrode materials for supercapacitor. As a comparison, the performance of the commercially available Co_3O_4 nanoparticles was also measured, which was noted as Co_3O_4-com (Figure S3b). The detailed structural parameters of Co_3O_4 are listed in Table 1.

Table 1. Summary of Structural Information of Co_3O_4 and Their OER Electrocatalytic Activities in pH 14 KOH

sample	BET (m^2/g)	η @ 10 mA/cm^2	η @ 20 mA/cm^2	η @ 50 mA/cm^2	η @ 100 mA/cm^2	current density @ 0.8 V vs Ag/AgCl	TOF (s^{-1}) @ 400 mV overpotential
$Co(OH)_2$	328.6	422	450	502	561	134.3	4.97×10^{-3}
HFC-250	245.5	409	431	467	500	404.8	1.67×10^{-2}
HFC-400	67.3	426	458	507	565	131.1	1.51×10^{-2}
Co_3O_4-com	4.12					7.9	3.1×10^{-4}

DOI: 10.1021/acsami.5b05989
ACS Appl. Mater. Interfaces 2015, 7, 20322−20331

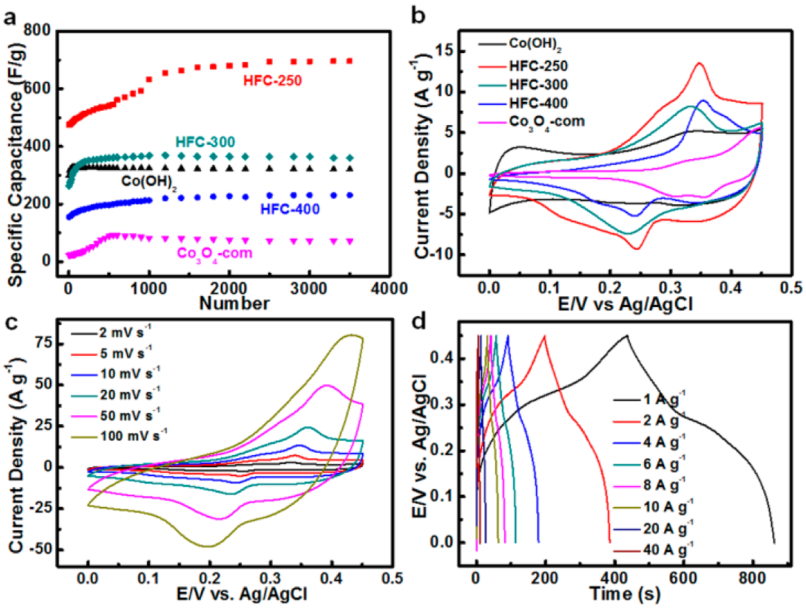

Figure 2. (a) Cyclability of the $Co(OH)_2$, HFC-250, HFC-300, HFC-400, and Co_3O_4-com electrodes upon charge−discharge at a current density of 10 A g^{-1}. (b) CV curves of the $Co(OH)_2$ cage and the HFC-250, HFC-300, HFC-400, and Co_3O_4-com electrodes at a scan rate of 10 mV s^{-1}. (c) CV curves of the HFC-250 electrode at various scan rates (2, 5, 10, 20, 50, and 100 mV s^{-1}). (d) Charge−discharge profiles of the HFC-250 electrodes at different current densities.

As the electroactive candidates for supercapacitors, it is well-known that the Co_3O_4 materials usually undergo an activation process at the electrode−electrolyte interface.[46,47] In this work, the electroactivity of the HFC Co_3O_4 electrodes is also evaluated by the charge−discharge process measured at constant current density of 10 A g^{-1} within a voltage window from 0 to 0.45 V in 2 M KOH electrolyte. As shown in Figure 2a, the activation processes for the HFC Co_3O_4 electrodes and Co_3O_4-com electrode were indeed observed. The electrochemical performance was recorded until the electrode materials were fully activated.

The electrochemical performance of the HFC $Co(OH)_2$ and Co_3O_4 electrode materials was investigated by CV in a three-electrode cell in 2.0 M KOH electrolyte solution. Figure 2b presents representative CV curves measured in a 2.0 M KOH solution at a scan rate of 10 mV s^{-1} for $Co(OH)_2$, HFC-250, HFC-300, HFC-400, and Co_3O_4-com. It can be clearly observed that there is a distinct pair of redox peaks during the anodic and cathodic sweeps, with a broad redox background. The asymmetrical CV curves are consistent with the previous studies on the cobalt-based electrodes in aqueous KOH electrolyte and suggest that the capacitance characteristic of the electroactive materials mainly originated from the pseudocapacitive capacitance of Co_3O_4.[47−49] The redox peaks correspond to the reversible conversion between different cobalt oxidation states. In the case of oxidation, the two sequential reactions are described as follows.[34,35,50]

$$Co_3O_4 + H_2O + OH^- \rightarrow 3CoOOH + e^- \qquad (4)$$

or

$$Co(OH)_2 + OH^- \rightarrow 3CoOOH + H_2O + e^- \qquad (5)$$

$$CoOOH + OH^- \rightarrow CoO_2 + H_2O + e^- \qquad (6)$$

The integrated areas derived from CV curves of the HFC Co(OH) and Co_3O_4 were significantly larger than that of the Co_3O_4-com electrode, which demonstrated that HFC with large surface areas could improve the electrochemical performance in the presence of a large amount of surface active sites. Among of them, HFC-250 exhibited the largest CV curve area, indicating that the HFC-250 electrode possessed the highest specific capacitance. This could be ascribed to the structural features of HFC-250 for the favorable chemical and charge transfer and the large amount of the available surface active cobalt species involving the redox reactions. Figure 2c shows the representative CV curves of the HFC-250 electrode at various scan rates from 2 to 100 mV s^{-1}. Accompanied by the increase of the scan rate, the anodic peak potential was shifted to a higher value, and the cathodic peak potential was shifted to the lower value, which could be attributed to the polarization of the electrode under a high scan rate. Besides, the peak current densities increased with the increase of the scan rates, indicating the rapid reversible redox reaction of the electrode materials. Similar electro-behavior was also observed for the HFC $Co(OH)_2$, HFC-300, HFC-400, and Co_3O_4-com electrodes from their CV curves at various scan rates from 2 to 100 mV s^{-1} (Figure S4).

For further insight into the capacitive property of the HFC-$Co(OH)_2$, HFC-250, HFC-300, HFC-400, and Co_3O_4-com electrode materials, the galvanostatic charge−discharge measurements were carried out in 2 M KOH electrolyte between 0 and 0.45 V (vs Ag/AgCl) at various current densities ranging from 1 to 40 A g^{-1}, as shown in Figures 2d and S4. The nearly symmetric potential−time curves at various current densities (Figure 2d) imply that the HFC-250 electrode delivers a high charge−discharge Coulombic efficiency and a low polarization. The specific capacitance can be calculated according to the following equation[37,39,46]

$$C = \frac{I \times \Delta t}{m \times \Delta V} \qquad (7)$$

where C (F g^{-1}) is the specific capacitance, I (mA) is the discharge current, Δt (s) is the discharge time, ΔV (V) is the potential change during the discharge process, and m (mg) is

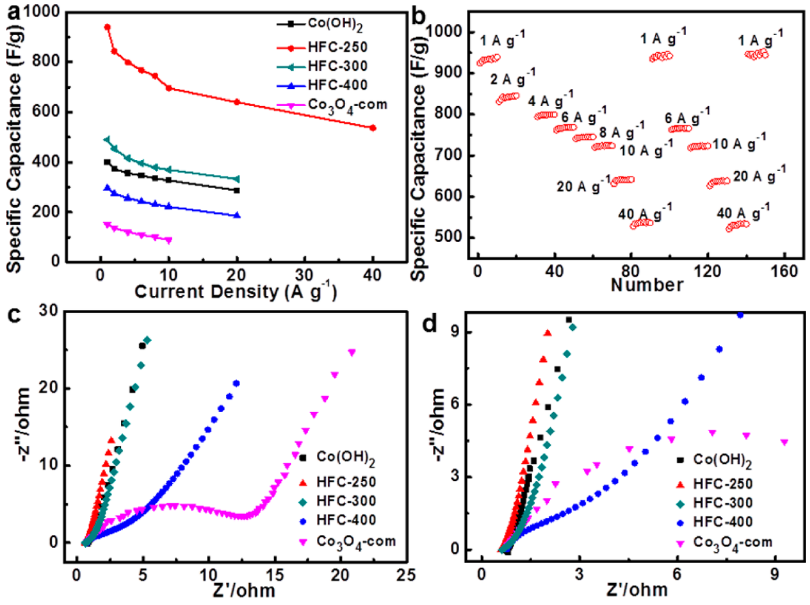

Figure 3. (a) Plots of specific capacitance of Co(OH)$_2$, HFC-250, and HFC-400 as a function of current density. (b) Rate capability of the HFC-250 electrode upon progressively varying the current density. (c and d) Impedance Nyquist plots of the Co(OH)$_2$, HFC-250, HFC-300, HFC-400, and Co$_3$O$_4$-com electrodes. The measurements were recorded after 3500 cycles for all electrodes.

the weight of electroactive material within the electrode. The specific capacitance values of HFC-250 calculated from the discharge curves are 948.9, 843.2, 798.3, 768.5, 744.9, 723.5, 640.8, and 536.8 F g^{-1} at the charge−discharge current densities of 1, 2, 4, 6, 8, 10, 20, and 40 A g^{-1}, respectively. The decreased capacitances with the increase of the discharge current densities could be attributed to the resistance increase of Co$_3$O$_4$ and the relatively insufficient faradic redox reactions at high current densities.[46] It is worthwhile to note that these capacitive values of HFC-250 are among the best performance for cobalt-based electroactive materials and even better than some of the composites of cobalt oxides and conductive frameworks as summarized in Table S1.

To compare with other samples (Co(OH)$_2$, HFC-300, HFC-400, and Co$_3$O$_4$-com), the specific capacitances of each electrode at various current densities are summarized in Figure 3a. At each current density, the derived specific capacitance of the HFC-250 electrodes is much larger than those of other electrodes (Co(OH)$_2$, HFC-300, HFC-400, and Co$_3$O$_4$-com). Taking the current density of 1 A g^{-1} as an example, HFC-250 electrode possesses the largest specific capacitance of 948.9 F g^{-1}, which is 1.94, 2.37, and 3.19 times higher than those for the HFC-300 (489.9 F g^{-1}), HFC Co(OH)$_2$ (400.7 F g^{-1}), and HFC-400 (297 F g^{-1}) electrodes, respectively. All HFC electrodes deliver much larger capacitances than that of the Co$_3$O$_4$-com electrode (151.3 F g^{-1}), consistent with the CV curves in Figure 2b. The above results clearly indicate that HFC-250 can deliver superior specific capacitance.

Generally, a good electrochemical supercapacitor is expected to provide high energy density or high specific capacitances at high current densities. Impressively, the specific capacitance of HFC-250 is 536.8 F g^{-1} at a high current density of 40 A g^{-1}, equivalent to 56.6% retention of the capacitive value at 1 A g^{-1}. To our knowledge, the extrusive performance of HFC-250 as the electroactive materials for supercapacitors operated at such a high current density is the first demonstrated example for cobalt oxides in the absence of any conductive framework. The performance of HFC-250 is even better some of the composites of cobalt oxides and conductive supports as summarized in Table S2. The electrochemical results described above unambiguously suggest the potential applications of HFC-250 for a high-power density operation.

Cycliability of the electroactive materials is another important indicator of the performance for a supercapacitor. The long-term cycling performance of the HFC-250, HFC-400, and Co(OH)$_2$ electrodes was measured at a constant current density of 10 A g^{-1} as shown in Figures 2a and S5. No capacitance loss was observed for HFC-250 during 10 000 cycles (Figure S5), suggesting its superior electrochemical stability for supercapacitors. The microstructures of HFC-250 after cycling were also characterized by TEM as shown in Figure S6. Despite the broken cages observed, the preservation of the cage-like morphology benefits the charge conductivity and chemical diffusion. The electrodes of Co(OH)$_2$, HFC-300, HFC-400, and Co$_3$O$_4$-com also exhibit a remarkable stability as the electroactive materials for supercapacitors (Figure 2a). However, their potential applications are limited because of their much smaller specific capacitances.

Figure 3b demonstrates the superior rate capability of the HFC-250 electrode. After 3500 cycles at the current density of 10 A g^{-1}, 10 charge/discharge cycles at various current densities were carried out for the same electrode. The specific capacitance of the electrode at 1 A g^{-1} was completely reverted back to the initial values at 1 A g^{-1} after measurements at various current densities, as shown in Figure 3b. The same results were also observed for the HFC-250 electrode operated at other current densities, suggesting an outstanding rate capability of the HFC-250 electrodes reversibly operated at various current densities up to 40 A g^{-1}.

Apparently, the superior electrochemical properties of HFC-250 can be ascribed to its unique morphological features as shown in Figure 1. First of all, the HFC-like nanostructures reduce amount of the grain boundary and increase the charge conductivity of the electrodes. The more detailed characteristics of the capacitive electrode can be investigated with the electrochemical impedance spectroscopy (EIS). Typical Nyquist plots for the $Co(OH)_2$, HFC-250, HFC-300, HFC-400, and Co_3O_4-com electrodes are presented in Figure 3c. The impedance measurements of the electrodes were carried out after 3500 cycles. From the point intersecting with the real axis in the range of high frequency, the internal resistances of the HFC-250, HFC-300, HFC-400, and $Co(OH)_2$ were approximately 0.58, 0.67, 0.75, and 0.71 Ω, respectively. However, the Co_3O_4-com electrode showed a bigger resistance (13.2 Ω). The results demonstrated that the lowest value of HFC-250 indicated the best charge conductivity of the electrode fabricated from HFC-250. The hollow fluffy feature of HFC-250, HFC-400, and $Co(OH)_2$ is a cage-like structure constructed by the ultrathin nanosheets with large interior voids, which can significantly increase the chemical diffusion of the electrodes as a consequence. Similar phenomena have been reported for hollow Co_3O_4 structures for energy storage.[28−30] In the low-frequency ranges of Nyquist plots, the straight line corresponds to the Warburg resistance relative to the diffusion of the electrolyte within the electroactive materials.[44,51] As shown in Figure 3d, the slopes of all electrodes are larger than 45°, indicating the efficient chemical diffusion for all electrodes. However, from TEM images of HFC Co_3O_4 (Figures 1, S1, and S3), the collapsed structures of HFC-400 largely reduce the available surface area for interaction with electrolyte and block the opening pores of the cage compared with the structure of HFC-250, which may decrease the accessibility of the electrolyte within the HFC-400 electrodes. This also can be revealed by the pore size distribution of the HFC structures (Figure S7). The pores created by nanosheets for HFC-250 are generally larger than 20 nm. In contrast, many small pores below 15 nm for HFC-300 and HFC-400 are observed because of the collapsed structures under the high-temperature treatments, which will decrease the chemical diffusion process.

Moreover, the HFC constructed by the ultrathin nanosheets provide large surface areas and more catalytic sites for the surface redox reactions. The surface area of HFC-250 is 2.05, 3.65, and 59.6 times larger than that of HFC-300, HFC-400, and Co_3O_4-com, respectively, indicating the higher catalytic activity of HFC-250 as the electroactive materials for supercapacitors. Although the surface area of HFC $Co(OH)_2$ is larger than that of HFC-250, its low electrochemical performance can be ascribed to the less active surface and relative low conductivity of the HFC $Co(OH)_2$ electrodes. Moreover, the thinness of nanosheets of HFC-250 indicates the higher catalytic activity due to the low-coordinated surface cobalt species. In contrast, the morphology of HFC-400 (Figure S3a) presents the melting-like behavior of the nanosheets under the higher-temperature annealing. Thus, it increased the thickness of cage and reduced the catalytic activity of surface cobalt species for the HFC-400 electrodes.

The energy density (E) and power density (P) are the two major factors for evaluating the applications of the electrochemical supercapacitors. We calculated the energy density and power density according to previous reports,[26,52] and the details are shown in Supporting Information. The HFC-250 elecrodes delivered a high energy density of 26.5 Wh kg^{-1} at a specific power density of 37.3 kW kg^{-1}, which was much larger than that of HFC-$Co(OH)_2$ (10.4 Wh kg^{-1}) and Co_3O_4-com (3.84 Wh kg^{-1}). The HFC 250 electrodes also deliver higher energy density and power density than majority of cobalt-based devices.[36,41,53] Energy density (or power density) of the HFC-250 electrode is lower than some of them at a similar power density (or energy density), which was composited with the conductive materials such as the brush-like Co_3O_4 nanowires/carbon fiber paper,[41] CNT/MnO_2 composites,[54] $MnCo_2O_4$,[53] MnO_2/nanoporous gold,[52] and SWCNTs//RuO_2.[55] Considering the free-standing HFC, HFC-250 benefits from its structural features and represents a promising candidate for energy storage.

3.3. HFC Co_3O_4 for Oxygen Evolution Reaction.

As a promising candidate for the supercapacitors, HFC-250's unique structures benefit the chemical and charge transfer and possess the large fraction of surface cobalt species with a high catalytic activity for surface redox reactions, suggesting its potentials for many electroactive applications. The catalytic activity of cobalt oxides for oxygen evolution reaction (OER) also has been widely explored. According to previous studies,[56,57] the structural features of HFC-250 are expected to exhibit a high catalytic behavior toward OER.

To evaluate the OER activities of HFC-250, the catalysts were loaded onto an ITO electrode by drop casting. The catalyst loading was controlled at 0.14 mg cm^{-2} for all experiments. The OER catalytic activity of $Co(OH)_2$, HFC-250, HFC-400 and Co_3O_4-com was measured in pH 14.0 KOH solution. In this work, the potential for the anode $E°_{OH^-/O_2}$ = 0.404 V versus that of the normal hydrogen electrode (NHE) at pH 14.0 (0.206 V vs Ag/AgCl) was used to calculate the overpotentials for catalysts.[56,57] We have reported that ITO is inactive for water oxidation.[58] Figure 4a reveals the electrocatalytic activities of all samples for OER. The overpotentials of all catalysts at a specified current density (10, 20, 50, and 100 mA cm^{-2}) and the current densities observed at 0.8 V (vs Ag/AgCl) are summarized in Table 1. The overpotentials of the HFC-250 electrode at the current density of 10 mA cm^{-2} was 409 mV, which was 13 and 17 mV lower than those of the HFC $Co(OH)_2$ and HFC-400 electrodes, respectively. The same tendency was also observed for all electrodes at each current density. Moreover, the current density of 404.8 mA cm^{-2} for HFC-250 at 0.8 V (vs Ag/AgCl) was much larger than those of 134.3, 131.1, and 7.9 mA cm^{-2} for HFC $Co(OH)_2$, HFC-400, and Co_3O_4-com, respectively. These results demonstrated the HFC-250 can act as a very active electrocatalyst for oxygen evolution under an alkaline condition.

The concentration of electrolyte also has an important effect on the electrochemical catalytic activity of the catalysts for OER. Hence, the catalytic activity of the HFC-250 electrode was also evaluated in KOH electrolyte solutions with various pH values of 12.0 and 13.0. As given in Figure 4b, a low current density of 6.0 mA cm^{-2} at 0.8 V (vs Ag/AgCl) was observed for HFC-250 in pH 12.0 KOH. Increasing the concentration of KOH electrolyte with pH 13.0 and 14.0 gave much higher current densities of 65.3 and 404.8 mA cm^{-2}, respectively. The observation is very consistent with previous reports that raising the concentration of OH^- in the electrolyte can increase the OER activity of Co_3O_4 catalysts.[56,57]

The TOF for oxygen evolution can be calculated from the anodic current density, assuming 100% Faradaic efficiency and each Co atom as an active site (a lower bound on activity). At the overpotential of 400 mV, the TOF of 1.67×10^{-2} s^{-1} for HFC-250 in pH 14.0 KOH is much higher than those for $Co(OH)_2$ (4.97×10^{-3} s^{-1}) and HFC-400 (1.51×10^{-2} s^{-1}) under the same conditions (Figure 4c). The Co_3O_4-com electrode shows the lowest TOF value of 3.1×10^{-4} s^{-1} under the same conditions, indicating that HFCs possess catalytic activities better than that of Co_3O_4-com. Moreover, the

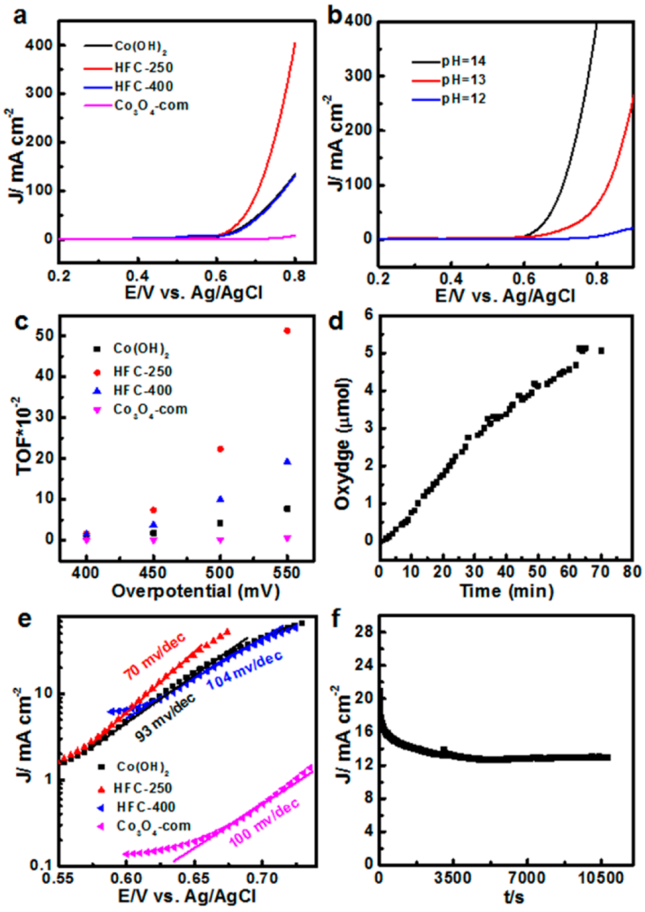

Figure 4. Electrochemical performance of Co(OH)$_2$, HFC-250, HFC-400, and Co$_3$O$_4$-com loaded on ITO electrodes. (a) Linear sweep voltammograms of all catalytic electrodes in pH 14 KOH with 95% iR corrections. The scanning rate was 50 mV/s. (b) Linear voltammograms of the HFC-250 electrode in KOH electrolyte solutions with various pH values with 95% iR corrections. (c) The derived TOF values of three catalysts at different overpotentials in pH 14 KOH electrolyte, assuming all Co atoms are active sites. (d) O$_2$ production measured by oxygen meter. (e) Tafel plots of all the catalysts loaded on ITO recorded in pH 14 KOH, corresponding to the LSV curves in panel a. (f) Chronoamperometric measurements of the HFC-250 biased at 0.7 V (vs Ag/AgCl) in pH 14 KOH at a scan rate of 10 mV s^{-1}.

calculated values of TOF of HFC-250 at high applied potentials become much larger than those of other Co$_3$O$_4$ catalysts at the same potential, as presented in Figure 4c. Considering more cobalt atoms inaccessible for the HFC-400 electrodes, the larger value of TOF for HFC-250 indicates the great catalytic activity of surface cobalt species of HFC-250 toward OER. The calculated TOF value of the HFC-250 catalysts is 1.07 × 10^{-2} s^{-1} at the overpotential of 400 mV in pH 13.0 KOH solution, which is far larger than that of mesoporous Co$_3$O$_4$-35 (4.55 × 10^{-3} s^{-1}) and other cobalt-based OER electrocatalysts under similar conditions.[16,56,57,59] The results further indicate that HFC-250 displays a high OER activity for the electrocatalytic water-splitting reaction and shows potential as efficient cocatalysts for photo-assisted water splitting. To further confirm the catalytic activity of HFC-250 toward OER, the reaction was monitored using an oxygen meter (Orion Star A213) in the airtight reactor. Before each measurement, the reaction solution was degassed with an argon flow until the concentration of the dissolved O$_2$ reached zero. After a 60 min reaction, the produced oxygen of the HFC-250 electrode (Figure 4d) reached up to 4.56 μmol at an applied voltage of 0.7 V (vs Ag/AgCl).

We also fit the polarization curves of HFC-250, Co(OH)$_2$, HFC-400, and Co$_3$O$_4$-com (Figure 4a) to the Tafel equation $\eta = b \log(j/j_0)$,[58,60] where η is the overpotential, b is the Tafel slope, j is the current density, and j_0 is the exchange current density. As presented in Figure 4e, the derived Tafel slope of 70 mV dec^{-1} for HFC-250 is much smaller than those for HFC-400 (104 mV dec^{-1}) and HFC Co(OH)$_2$ (93 mV dec^{-1}). The Tafel slope of HFC-250 is close to or even better than those reported for the reduced Co$_3$O$_4$ porous nanowires (72 mV dec^{-1}),[61] Co$_3$O$_4$ nanoparticles (78 mV dec^{-1}), Co$_3$O$_4$/graphene composites (68 mV dec^{-1}),[62] cobalt carbonate hydroxide/C (116 mV dec^{-1}),[63] and nanoporous hollow Co$_3$S$_4$ nanosheets (90 mV dec^{-1}),[64] suggesting the high OER activity of HFC-250. However, the value of the Tafel slope for HFC-250 is higher than those of binary metal oxides[65] and other materials,[66−68] which may be attributed to the introduction of the conductive supports for the growth of electroactive materials in previous reports.

The electrocatalytic activity of the HFC-like cobalt-based catalysts for OER described above clearly demonstrates that HFC-250 is a promising cocatalyst for water splitting. Generally, many factors, such as material synthesis methods, geometrical features of catalysts, catalyst-loading approaches, supports, and pH value of electrolyte solution, among others, can significantly affect their performance.[56,57] Herein, the hollow fluffy structure of HFC-250 constructed from ultrathin nanosheets improves the charge and chemical diffusion and provides a large surface area and more catalytic sites for OER, suggesting the high catalytic activity toward OER as expected and measured. The stability of HFC-250 toward OER was also evaluated by running chronoamperometric responses (*I*−*t*) at 0.7 V in a N$_2$-saturated pH 14.0 KOH solution (Figure 4f). During the measurements, the working electrode was continuously rotating at 1600 rpm to remove the generated oxygen bubbles. It was found that OER current density of HFC-250 was dropped initially and then stabilized at 12.3 mA cm^{-2} for a period of 3 h. The results further demonstrate that the HFC-250 is a promising OER catalyst with high activity and strong durability.

4. CONCLUSIONS

We have successfully demonstrated the electrochemical activity of the HFC-like Co$_3$O$_4$ as a potential candidate for supercapacitors as well as catalysts for OER. The nanostructures were prepared by templating against Cu$_2$O nanocrystals in the presence of Na$_2$S$_2$O$_3$ and cobalt precursor and subsequent thermal treatments. The Co$_3$O$_4$ HFCs annealed at 250 °C deliver a large surface area, provide more surface active sites for redox reaction, minimize the amount of the grain boundaries, and improve the charge and chemical diffusion. As the electroactive component for supercapacitors, the HFC-250 electrodes exhibit a superior rate capability in the range of 1.0−40 A g^{-1}, deliver a large specific capacitance of 948.9 F g^{-1} at a current density of 1 A g^{-1}, and show an excellent recycling stability during 10 000 cycles at a high current density of 10 A g^{-1}. Importantly, the high specific capacitance (536.8 F g^{-1}) of HFC-250 at 40 A g^{-1} suggests the potential application for high power density. OER catalytic studies demonstrate the highest catalytic activity of HFC-250 with the highest TOF (1.67 ×

10^{-2} s^{-1}, low bound) and the smallest Tafel slope (70 mV dec^{-1}). The high catalytic activity can be attributed to their structural features. The Co_3O_4 HFCs with efficient electrochemical catalytic activities and good stability are promising candidates for electrochemical energy conversion and storage.

■ ASSOCIATED CONTENT

Ⓢ Supporting Information

The Supporting Information is available free of charge on the ACS Publications website at DOI: 10.1021/acsami.5b05989.

> SEM and TEM images of hollow fluffy cages and the commercial Co_3O_4; electrochemical performance of HFC $Co(OH)_2$, HFC-300, HFC-400, and Co_3O_4-com; calculation for power density and energy density. (PDF)

■ AUTHOR INFORMATION

Corresponding Authors

*E-mail: yyma@mail.xjtu.edu.cn.
*E-mail: yongquan@mail.xjtu.edu.cn.

Author Contributions

X.Z. and X.S. contributed equally to this work.

Notes

The authors declare no competing financial interest.

■ ACKNOWLEDGMENTS

We acknowledge the financial support from a National Natural Science Foundation of China 21201138 and 21401148. This work was also partially funded by the Ministry of Science and Technology of China through a 973-program under Grant 2012CB619401 and supported by the Fundamental Research Funds for the Central Universities (xjj2013102 and xjj2013043). Technical support for TEM experiments from Frontier Institute of Science and Technology and SEM experiments from State Key Laboratory for Manufacturing Systems Engineering, Xi'an Jiaotong University, are also acknowledged.

■ REFERENCES

(1) Wang, H. L.; Dai, H. J. trongly Coupled Inorganic-nano-carbon Hybrid Materials for Energy Storage. *Chem. Soc. Rev.* **2013**, *42*, 3088−3113.

(2) Qu, Y.; Duan, X. F. Progress, Challenge and Perspective of Heterogeneous Photocatalysts. *Chem. Soc. Rev.* **2013**, *42*, 2568−2580.

(3) Qu, Y.; Duan, X. F. One-dimensional Homogeneous and Heterogeneous Nanowires for Solar Energy Conversion. *J. Mater. Chem.* **2012**, *22*, 16171−16181.

(4) Naoi, K.; Naoi, W.; Aoyagi, S.; Miyamoto, J. I.; Kamino, T. New Generation "Nanohybrid Supercapacitor. *Acc. Chem. Res.* **2013**, *46*, 1075−1083.

(5) Zhao, X.; Sanchez, B. M.; Dobson, P. J.; Grant, P. S. The Role of Nanomaterials in Redox-based Supercapacitors for Next Generation Energy Storage Devices. *Nanoscale* **2011**, *3*, 839−855.

(6) Reddy, A. L. M.; Gowda, S. R.; Shaijumon, M. M.; Ajayan, P. M. Hybrid Nanostructures for Energy Storage Applications. *Adv. Mater.* **2012**, *24*, 5045−5064.

(7) Simon, P.; Gogotsi, Y. Materials for Electrochemical Capacitors. *Nat. Mater.* **2008**, *7*, 845−854.

(8) Nocera, D. G. The Artificial Leaf. *Acc. Chem. Res.* **2012**, *45*, 767−776.

(9) Wang, G. P.; Zhang, L.; Zhang, J. J. A Review of Electrode Materials for Electrochemical Supercapacitors. *Chem. Soc. Rev.* **2012**, *41*, 797−828.

(10) Wei, W. F.; Cui, X. W.; Chen, W. X.; Ivey, D. G. Manganese Oxide-based Materials as Electrochemical Supercapacitor Electrodes. *Chem. Soc. Rev.* **2011**, *40*, 1697−1721.

(11) Fan, Z. J.; Yan, J.; Wei, T.; Zhi, L. J.; Ning, G. Q.; Li, T. Y.; Wei, F. Asymmetric Supercapacitors Based on Graphene/MnO_2 and Activated Carbon Nanofiber Electrodes with High Power and Energy Density. *Adv. Funct. Mater.* **2011**, *21*, 2366−2375.

(12) Chen, X. A.; Chen, X. H.; Zhang, F. Q.; Yang, Z.; Huang, S. M. One-pot Hydrothermal Synthesis of Reduced Graphene Oxide/carbon Nanotube/a-$Ni(OH)_2$ Composites for High Performance Electrochemical Supercapacitor. *J. Power Sources* **2013**, *243*, 555−561.

(13) Zhong, D. K.; Sun, J. W.; Inumaru, H.; Gamelin, D. R. Reactive Ballistic Deposition of α-Fe_2O_3 Thin Films for Photoelectrochemical Water Oxidation. *J. Am. Chem. Soc.* **2009**, *131*, 6086−6087.

(14) Kanan, M. W.; Surendranath, Y.; Nocera, D. G. Cobalt-phosphate Oxygen-evolving Compound. *Chem. Soc. Rev.* **2009**, *38*, 109−114.

(15) Jiao, F.; Frei, H. Nanostructured Cobalt Oxide Clusters in Mesoporous Silica as Efficient Oxygen-evolving Catalysts. *Angew. Chem., Int. Ed.* **2009**, *48*, 1841−1844.

(16) Rosen, J.; Hutchings, G. S.; Jiao, F. Ordered Mesoporous Cobalt Oxide as Highly Efficient Oxygen Evolution Catalyst. *J. Am. Chem. Soc.* **2013**, *135*, 4516−4521.

(17) Subbaraman, R.; Tripkovic, D.; Chang, K. C.; Strmcnik, D.; Paulikas, A. P.; Hirunsit, P.; Chan, M.; Greeley, J.; Stamenkovic, V.; Markovic, N. M. Trends in Activity for The Water Electrolyser Reactions on 3d M(Ni,Co,Fe,Mn) Hydr(oxy)oxide Catalysts. *Nat. Mater.* **2012**, *11*, 550−557.

(18) Smith, R. D.; Prevot, M. S.; Fagan, R. D.; Trudel, S.; Berlinguette, C. P. Water Oxidation Catalysis: Electrocatalytic Response to Metal Stoichiometry in Amorphous Metal Oxide Films Containing Iron, Cobalt, and Nickel. *J. Am. Chem. Soc.* **2013**, *135*, 11580−11586.

(19) Zhou, X. M.; Xia, Z. M.; Tian, Z. M.; Ma, Y. Y.; Qu, Y. Ultrathin Porous Co_3O_4 Nanoplates as Highly Efficient Oxygen Evolution Catalysts. *J. Mater. Chem. A* **2015**, *3*, 8107−8114.

(20) Li, Y. G.; Tan, B.; Wu, Y. Y. Mesoporous Co_3O_4 Nanowire Arrays for Lithium Ion Batteries with High Capacity and Rate Capability. *Nano Lett.* **2008**, *8*, 265−270.

(21) Kim, Y. J.; Lee, J. H.; Cho, S.; Kwon, Y.; In, I.; Lee, J.; You, N. H.; Reichmanis, E.; Ko, H.; Lee, K. T.; Kwon, H. K.; Ko, D. H.; Yang, H.; Park, B. Additive-Free Hollow-Structured Co_3O_4 Nanoparticle Li-Ion Battery. *ACS Nano* **2014**, *8*, 6701−6712.

(22) Xu, Y. X.; Huang, X. Q.; Lin, Z. Y.; Zhong, X.; Huang, Y.; Duan, X. F. One-step Strategy to Graphene/$Ni(OH)_2$ Composite Hydrogels as Advanced Three-dimensional Supercapacitor Electrode Materials. *Nano Res.* **2013**, *6*, 65−76.

(23) Xu, Y. X.; Lin, Z. Y.; Huang, X. Q.; Liu, Y.; Huang, Y.; Duan, X. F. Flexible Solid-State Supercapacitors Based on Three-Dimensional Graphene Hydrogel Films. *ACS Nano* **2013**, *7*, 4042−4049.

(24) Peng, C. X.; Chen, B. D.; Qin, Y.; Yang, S. H.; Li, C. Z.; Zuo, Y. H.; Liu, S. Y.; Yang, J. H. Facile Ultrasonic Synthesis of CoO Quantum Dot Graphene Nanosheet Composites with High Lithium Storage Capacity. *ACS Nano* **2012**, *6*, 1074−1081.

(25) Qiu, Y. C.; Chen, W.; Yang, S. H. Double-Layered Photoanodes from Variable-Size Anatase TiO_2 Nanospindles: A Candidate for High-Efficiency Dye-Sensitized Solar Cells. *Angew. Chem., Int. Ed.* **2010**, *49*, 3675−3679.

(26) Mai, L. Q.; Li, H.; Zhao, Y. L.; Xu, L.; Xu, X.; Luo, Y. Z.; Zhang, Z. F.; Ke, W.; Niu, C. J.; Zhang, Q. J. Fast Ionic Diffusion-Enabled Nanoflake Electrode by Spontaneous Electrochemical Pre-Intercalation for High-Performance Supercapacitor. *Sci. Rep.* **2013**, *3*, 1078−1085.

(27) Hercule, K. M.; Wei, Q. L.; Khan, A. M.; Zhao, Y. L.; Tian, X. C.; Mai, L. Q. Synergistic Effect of Hierarchical Nanostructured $MoO_2/Co(OH)_2$ with Largely Enhanced Pseudocapacitor Cyclability. *Nano Lett.* **2013**, *13*, 5685−5691.

(28) Wang, X.; Wu, X. L.; Guo, Y. G.; Zhong, Y. T.; Cao, X. Q.; Ma, Y.; Yao, J. N. Synthesis and Lithium Storage Properties of Co_3O_4

Nanosheet-Assembled Multishelled Hollow Spheres. *Adv. Funct. Mater.* **2010**, *20*, 1680−1686.

(29) Wang, X.; Tian, W.; Zhai, T. Y.; Zhi, C. Y.; Bando, Y.; Golberg, D. Cobalt(II,III) Oxide Hollow Structures: Fabrication, Properties and Applications. *J. Mater. Chem.* **2012**, *22*, 23310−23326.

(30) Wang, X.; Yu, L. J.; Wu, X. L.; Yuan, F. L.; Guo, Y. G.; Ma, Y.; Yao, J. N. Synthesis of Single-Crystalline Co_3O_4 Octahedral Cages with Tunable Surface Aperture and Their Lithium Storage Properties. *J. Phys. Chem. C* **2009**, *113*, 15553−15558.

(31) Yuan, C. Z.; Yang, L.; Hou, L. R.; Shen, L. F.; Zhang, F.; Li, D.; Zhang, X. G. Large-scale Co_3O_4 Nanoparticles Growing on Nickel Sheets via a One-step Strategy and Their Ultra-highly Reversible Redox Reaction toward Supercapacitors. *J. Mater. Chem.* **2011**, *21*, 18183−18185.

(32) Wang, G. X.; Shen, X. P.; Horvat, J.; Wang, B.; Liu, H.; Wexler, D.; Yao, J. Hydrothermal Synthesis and Optical, Magnetic, and Supercapacitance Properties of Nanoporous Cobalt Oxide Nanorods. *J. Phys. Chem. C* **2009**, *113*, 4357−4361.

(33) Cui, L.; Li, J.; Zhang, X. G. Preparation and properties of Co_3O_4 nanorods as supercapacitor material. *J. Appl. Electrochem.* **2009**, *39*, 1871−1876.

(34) Gao, Y. Y.; Chen, S. L.; Cao, D. X.; Wang, G. L.; Yin, J. L. Electrochemical Capacitance of Co_3O_4 Nanowire Arrays Supported on Nickel Foam. *J. Power Sources* **2010**, *195*, 1757−1760.

(35) Xia, X. H.; Tu, J. P.; Mai, Y. J.; Wang, X. L.; Gu, C. D.; Zhao, X. B. Self-supported Hydrothermal Synthesized Hollow Co_3O_4 Nanowire Arrays with High Supercapacitor Capacitance. *J. Mater. Chem.* **2011**, *21*, 9319−9325.

(36) Xia, X. H.; Tu, J. P.; Zhang, Y. Q.; Mai, Y. J.; Wang, X. L.; Gu, C. D.; Zhao, X. B. Freestanding Co_3O_4 Nanowire Array for High Performance Supercapacitors. *RSC Adv.* **2012**, *2*, 1835−1841.

(37) Xiong, S. L.; Yuan, C. Z.; Zhang, X. G.; Xi, B. J.; Qian, Y. T. Controllable Synthesis of Mmesoporous Co_3O_4 Nanostructures with Tunable Morphology for Application in Supercapacitors. *Chem. - Eur. J.* **2009**, *15*, 5320−5326.

(38) Lu, Z. Y.; Yang, Q.; Zhu, W.; Chang, Z.; Liu, J. F.; Sun, X. M.; Evans, D. G.; Duan, X. One-step Strategy to Graphene/$Ni(OH)_2$ Composite Hydrogels as Advanced Three-dimensional Supercapacitor Electrode Materials. *Nano Res.* **2012**, *5*, 369−378.

(39) Zhu, T.; Chen, J. S.; Lou, X. W. Shape-controlled Synthesis of Porous Co_3O_4 nanostructures for Application in Supercapacitors. *J. Mater. Chem.* **2010**, *20*, 7015−7020.

(40) Li, Y. H.; Huang, K. L.; Liu, S. Q.; Yao, Z. F.; Zhuang, S. X. Meso-macroporous Co_3O_4 Electrode Prepared by Polystyrene Spheres and Carbowax Templates for Supercapacitors. *J. Solid State Electrochem.* **2011**, *15*, 587−592.

(41) Rakhi, R. B.; Chen, W.; Cha, D.; Alshareef, H. N. Substrate Dependent Self-organization of Mesoporous Cobalt Oxide Nnanowires with Remarkable Pseudocapacitance. *Nano Lett.* **2012**, *12*, 2559−2567.

(42) Guan, C.; Liu, J. P.; Cheng, C. W.; Li, H. X.; Li, X. L.; Zhou, W. W.; Zhang, H.; Fan, H. J. Hybrid Structure of Cobalt Monoxide Nanowire @ nickel Hydroxidenitrate Nanoflake Aligned on Nickel Foam for High-rate Supercapacitor. *Energy Environ. Sci.* **2011**, *4*, 4496−4499.

(43) Cao, Y. B.; Yuan, F. L.; Yao, M. S.; Bang, J. H.; Lee, J. H. A New Synthetic Route to Hollow Co_3O_4 Octahedra for Supercapacitor Applications. *CrystEngComm* **2014**, *16*, 826−833.

(44) Xiao, Y. H.; Liu, S. J.; Li, F.; Zhang, A. Q.; Zhao, J. H.; Fang, S. M.; Jia, D. Z. 3D Hierarchical Co_3O_4 Twin-Spheres with an Urchin-Like Structure: Large-Scale Synthesis, Multistep-Splitting Growth, and Electrochemical Pseudocapacitors. *Adv. Funct. Mater.* **2012**, *22*, 4052−4059.

(45) Nai, J. W.; Tian, Y.; Guan, X.; Guo, L. Pearson's Principle Inspired Generalized Strategy for the Fabrication of Metal Hydroxide and Oxide Nanocages. *J. Am. Chem. Soc.* **2013**, *135*, 16082−16091.

(46) Meng, F. L.; Fang, Z. G.; Li, Z. X.; Xu, W. W.; Wang, M. J.; Liu, Y. P.; Zhang, J.; Wang, W. R.; Zhao, D. Y.; Guo, X. H. Porous Co_3O_4 Materials Prepared by Solid-state Thermolysis of a Novel Co-MOF Crystal and Their Superior Energy Storage Performances for Supercapacitors. *J. Mater. Chem. A* **2013**, *1*, 7235−7241.

(47) Dong, X. C.; Xu, H.; Wang, X. W.; Huang, Y. X.; Chan-Park, M. B.; Zhang, H.; Wang, L. H.; Huang, W.; Chen, P. 3D Graphene-Cobalt Oxide Electrode for High-Performance Supercapacitor and Enzymeless Glucose Detection. *ACS Nano* **2012**, *6*, 3206−3213.

(48) Kung, C. W.; Chen, H. W.; Lin, C. Y.; Vittal, R.; Ho, K. C. Synthesis of Co_3O_4 Nanosheets via Electrodeposition Followed by Ozone Treatment and Their Application to High-performance Supercapacitors. *J. Power Sources* **2012**, *214*, 91−99.

(49) Du, W.; Liu, R. M.; Jiang, Y. W.; Lu, Q. Y.; Fan, Y. Z.; Gao, F. Facile Synthesis of Hollow Co_3O_4 Boxes for High Capacity Supercapacitor. *J. Power Sources* **2013**, *227*, 101−105.

(50) Meher, S. K.; Rao, G. R. Ultralayered Co_3O_4 for High-Performance Supercapacitor Applications. *J. Phys. Chem. C* **2011**, *115*, 15646−15654.

(51) Xiao, Y. H.; Zhang, A. Q.; Liu, S. J.; Zhao, J. H.; Fang, S. M.; Jia, D. Z.; Li, F. Free-standing and Porous Hierarchical Nanoarchitectures Constructed with Cobalt Cobaltite Nanowalls for Supercapacitors with High Specific Capacitances. *J. Power Sources* **2012**, *219*, 140−146.

(52) Lang, X. Y.; Hirata, A.; Fujita, T.; Chen, M. W. Nanoporous Metal/oxide Hybrid Electrodes for Electrochemical Supercapacitors. *Nat. Nanotechnol.* **2011**, *6*, 232−236.

(53) Yan, J.; Fan, Z. J.; Wei, T.; Cheng, J.; Shao, B.; Wang, K.; Song, L. P.; Zhang, M. L. Carbon Nanotube/MnO_2 Composites Synthesized by Microwave-assisted Method for Supercapacitors with High Power and Energy Densities. *J. Power Sources* **2009**, *194*, 1202−1207.

(54) Gomez, J.; Kalu, E. E. High-performance Binder-free Co-Mn Composite Oxide Supercapacitor Electrode. *J. Power Sources* **2013**, *230*, 218−224.

(55) Chen, P. C.; Chen, H.; Qiu, J.; Zhou, C. W. Inkjet Printing of Single-walled Carbon Nanotube/RuO_2 Nanowire Supercapacitors on Cloth Fabrics and Flexible Substrates. *Nano Res.* **2010**, *3*, 594−603.

(56) Esswein, A. J.; McMurdo, M. J.; Ross, P. N.; Bell, A. T.; Tilley, T. D. Size-Dependent Activity of Co_3O_4 Nanoparticle Anodes for Alkaline Water Electrolysis. *J. Phys. Chem. C* **2009**, *113*, 15068−15072.

(57) Tüysüz, H.; Hwang, Y. J.; Khan, S. B.; Asiri, A. M.; Yang, P. D. Mesoporous Co_3O_4 as an Electrocatalyst for Water Oxidation. *Nano Res.* **2013**, *6*, 47−54.

(58) Zhou, X. M.; Xia, Z. M.; Zhang, Z. Y.; Ma, Y. Y.; Qu, Y. One-step Synthesis of Multi-Walled Carbon nanotubes/ultra-thin $Ni(OH)_2$ Nanoplate Composite as Efficient Catalysts for Water Oxidation. *J. Mater. Chem. A* **2014**, *2*, 11799−11806.

(59) Yusuf, S.; Jiao, F. Effect of the Support on the Photocatalytic Water Oxidation Activity of Cobalt Oxide Nanoclusters. *ACS Catal.* **2012**, *2*, 2753−2760.

(60) Gong, M.; Li, Y. G.; Wang, H. L.; Liang, Y. Y.; Wu, J. Z.; Zhou, J. G.; Wang, J.; Regier, T.; Wei, F.; Dai, H. J. An Advanced Ni-Fe Layered Double Hydroxide Electrocatalyst for Water Oxidation. *J. Am. Chem. Soc.* **2013**, *135*, 8452−8455.

(61) Wang, Y. C.; Zhou, T.; Jiang, K.; Da, P. M.; Peng, Z.; Tang, J.; Kong, B.; Cai, W. B.; Yang, Z. Q.; Zheng, G. F. Reduced Mesoporous Co_3O_4 Nanowires as Efficient Water Oxidation Electrocatalysts and Supercapacitor Electrdes. *Adv. Energy Mater.* **2014**, *4*, 1400696.

(62) Liang, Y. Y.; Li, Y. G.; Wang, H. L.; Zhou, J. G.; Wang, J.; Regier, T.; Dai, H. J. Co_3O_4 Nanocrystals on Graphene as A Synergistic Catalyst for Oxygen Reduction Reaction. *Nat. Mater.* **2011**, *10*, 780−786.

(63) Wang, Y.; Ding, W.; Chen, S. G.; Nie, Y.; Xiong, K.; Wei, Z. D. Cobalt Carbonate Hydroxide/C: an Efficient Dual Electrocatalyst for Oxygen Reduction/Evolution Reactions. *Chem. Commun.* **2014**, *50*, 15529−15532.

(64) Zhao, W. W.; Zhang, C.; Geng, F. Y.; Zhuo, S. F.; Zhang, B. Nanoporous Hollow Transition Metal Chalcogenide Nanosheets Synthesized via the Anion-Exchange Reaction of Metal Hydroxides with Chalcogenide Ions. *ACS Nano* **2014**, *8*, 10909−10919.

(65) Song, F.; Hu, X. L. Ultrathin Cobalt-Manganese Layered Double Hydroxide Is an Efficient Oxygen Evolution Catalyst. *J. Am. Chem. Soc.* **2014**, *136*, 16481−16484.

(66) Zhang, Y. X.; Xiao, Q. Q.; Guo, X.; Zhang, X. X.; Xue, Y. F.; Jing, L.; Zhai, X.; Yan, Y. M.; Sun, K. N. A Novel Electrocatalyst for Oxygen Evolution Reaction Based on Rational Anchoring of Cobalt Carbonate Hydroxide Hydrate on Multiwall Carbon Nanotubes. *J. Power Sources* **2015**, *278*, 464−472.

(67) Wu, L. H.; Li, Q.; Wu, C. H.; Zhu, H. Y.; Mendoza-Garcia, A.; Shen, B.; Guo, J. H.; Sun, S. H. Stable Cobalt Nanoparticles and Their Monolayer Array as an Efficient Electrocatalyst for Oxygen Evolution Reaction. *J. Am. Chem. Soc.* **2015**, *137*, 7071−7074.

(68) Chang, Y. Q.; Antonietti, M.; Fellinger, T. P. Synthesis of Nanostructured Carbon through Ionothermal Carbonization of Common Organic Solvents and Solutions. *Angew. Chem., Int. Ed.* **2015**, *54*, 5507−5512.